Journal of Alloys and Compounds 488 (2009) 72–78

Contents lists available at ScienceDirect

Journal of Alloys and Compounds

journal homepage: www.elsevier.com/locate/jallcom

Hydrogen solubilities and permeabilities in un-oxidized and partially internally oxidized fcc Pd–Fe and $(Pd_{0.77}Ag_{0.23})_{1-x}Fe_x$ alloys (393–523 K)

Ted B. Flanagan*, D. Wang

Material Science Program and Department of Chemistry, University of Vermont, Burlington, VT 05405, USA

ARTICLE INFO

Article history:
Received 8 July 2009
Received in revised form 19 August 2009
Accepted 20 August 2009
Available online 31 August 2009

Keywords:
Thermodynamics
H diffusion
Pd–Fe alloys

ABSTRACT

Hydrogen solubilities have been measured for a series of Pd–Fe alloys in the temperature range from 393 to 523 K. From these equilibrium data the standard partial thermodynamic parameters at infinite dilution of H, ΔH°_{H} and ΔS°_{H} have been obtained and the former becomes less negative, and the latter more negative, with increase of X_{Fe}. H diffusion parameters have been determined in the Pd–Fe alloys (393–523 K). D_H decreases and E_D increases with X_{Fe} while the pre-exponential factors D°_{H} do not change significantly. The dependence of D_H and E_D on H content have been determined for several of the Pd–Fe alloys and the former decreases and the latter increases with the H contents.

1. Introduction

There have been many investigations of the solubility and thermodynamics of H_2 in Pd alloys and some general patterns of behavior have emerged[1]. Solid solution Pd alloys with expanded lattices such as Pd–Ag, Pd–Au, dissolve H_2 more exothermically than Pd and, consequently, the dilute phase solubilities are greater at a given p_{H_2} for these alloys than for Pd. Contracted alloys, which dissolve H_2 more endothermically than Pd, e.g., Pd–Ni, Pd–Rh, dissolve less H in the dilute phase at a given p_{H_2}. Substitution of Fe in the Pd lattice causes a contraction of the Pd lattice [2,3] which suggests [1] that ΔH°_{H} values should increase with X_{Fe} where the standard symbol refers to infinite dilution of H.

Hydrogen isotherms have been previously measured for Pd–Fe alloys near ambient temperature [4]. Some calorimetric determinations of the enthalpies of reaction of H_2 with the $Pd_{0.926}Fe_{0.074}$ and $Pd_{0.963}Fe_{0.037}$ alloys were also carried out in that work [4]. Dilute phase isotherms were determined earlier (273–342 K) by Flanagan et al. [5]. With regard to thermodynamic data for solution of H_2 at infinite dilution of H there appear to be conflicting results for Pd–Fe alloys [2,5]. One study [5] finds that ΔH°_{H} for H_2 absorption increases with X_{Fe} while the other [2] finds the opposite. The former is more consistent with the general trends for binary Pd alloys [1] and is also consistent with the observed decrease of solubility at a given p_{H_2} [5]. The two solid alloy-H phases, the dilute and hydride, disappear at about X_{Fe}=0.12 at room temperature according to [3].

In this work thermodynamic data will be determined from isotherms over a higher temperature range, 393–523 K, than investigated earlier [2,5] but this higher range will not affect the direction of the trends with X_{Fe} found at lower temperatures. These higher temperature data are needed to determine the dependence of diffusion parameters on H contents to be determined in this work.

Several papers have reported diffusion data in the ambient temperature range for H in Pd–Fe alloys [2,5–7]. McLellan and Yang [8] have questioned the diffusion results given by Sakamoto et al. [2] because the activation energies for diffusion which they report [2] do not extrapolate to the value for pure Pd at X_{Fe}=0 and their values of the pre-exponential factors, D°_{H}, are too small, e.g., 6.8×10^{-4} cm^2/s for a $Pd_{0.91}Fe_{0.09}$ alloy whereas for a similar composition McLellan and Yang find 1.24×10^{-2} cm^2/s. Both sets of results for D°_{H} appear anomalous. In this work the solubilities and diffusion parameters will be examined in part to resolve the discrepancies between these two sets of data [2,8].

It is known that D_H, Fick's diffusion constant, depends on the H concentration [9] and it has been shown recently that the permeation rates where p_{H_2} upstream, p_{up}, and downstream, p_{down}, are finite and 0, respectively, can be corrected for the non-ideality to obtain D^{*}_{H}, Einstein's concentration-independent diffusion constant [10]. D^{*}_{H} values will be obtained here using this approach.

The thermodynamic factor, $f(r)$, given by $(d\ln p^{1/2}/d\ln r)_T$ is needed to correct Fick's concentration-dependent diffusion constant, D_H, to Einstein's concentration-independent one, D^{*}_{H} [9], i.e.,

$$D_H = \frac{D^{*}_{H}(d\ln p^{1/2}/d\ln r)_T}{f_{cor}} = \frac{D^{*}_{H} f(r)}{f_{cor}} \quad (1)$$

* Corresponding author. Tel.: +1 802 656 0199; fax: +1 802 656 8705.
E-mail address: ted.flanagan@uvm.edu (T.B. Flanagan).

0925-8388/$ – see front matter © 2009 Elsevier B.V. All rights reserved.
doi:10.1016/j.jallcom.2009.08.113

where f_{cor} is the correlation factor and is $\leq$1.0 [11,12] and r =H-to-metal, atom ratio. Since the H concentrations employed are not large, it will be assumed here that $f_{cor} = 1.0$.

Under the present boundary conditions, $p_{upstream} > 0$ and $p_{downstream} = 0$, the degree of non-ideality due to the thermodynamic factor varies with H penetration through the membrane which can be allowed for using [10]

$$D_H = D_H^* \overline{f(r)} = \frac{D_H^* \left(\int_0^{r_{up}} f(r)dr\right)}{r_{up}} \quad (2)$$

where $\overline{f(r)}$ is the mean value of $f(r)$ over the membrane and, as noted, f_{cor} will be taken as 1.0.

In the 1980s McLellan and co-workers measured and collected data from the literature to show the general trends of D_H^* with X_M for H diffusion in several different fcc Pd-rich alloys where X_M is the atom fraction of alloying element M in Pd [6,13]. They found for most alloys that D_H^* decreased with increase of solute metal. They attributed the slowing to trapping of H by the solute metal. The solute metals Ag, Au and Ni did not decrease D_H^* very much as M increased from pure Pd(M = 0) which they attributed to anti-trapping [6]. More recently Züchner and coworkers [14] collected similar data and analyzed the results in terms of the prototype Pd–Ag system.

$(Pd_{0.77}Ag_{0.23})_{(1-x)}Fe_x$ alloys will also be investigated because the $Pd_{0.77}Ag_{0.23}$ alloy is the prime H purification membrane and the presence of small amounts of Fe will allow some partial internal oxidation (IO) which could lead to a greater resistance to gaseous poisons [15].

In the work to be reported here some of the alloy membranes were partially internally oxidized (IOed). Internal oxidation of a Pd–Fe alloy produces a composite Pd/Fe_2O_3 layer extending from the surface inwards. The oxide precipitates are nano-sized. It was shown earlier [16] that a novel way to determine whether the permeation is bulk diffusion controlled using only a single membrane is to measure steady state fluxes for different extents of IO at a given temperature and p_{H_2}. If the permeation is bulk diffusion controlled, there will be a linear relation between $1/J$ and the Pd layer thickness formed from the IO, i.e., $2d_{Pd}$ = fraction IO $\times$ d_o where d_{Pd} is the penetration depth of the IO and d_o is the initial membrane thickness. This method will be applied to the $Pd_{0.926}Fe_{0.074}$ and to two $(Pd_{0.77}Ag_{0.23})_{(1-x)}Fe_x$ alloy membranes. Results for the CO poisoning of these alloys will be reported elsewhere.

Fe is more oxidizable than Pd and therefore Pd–Fe alloys should be internally oxidizable forming small iron oxide precipitates within the Pd matrix. Recently Pd–Al alloys were internally oxidized to form Al_2O_3 precipitates within a Pd matrix [17]. Kirchheim and Huang et al. [18–20] studied the interaction of dissolved hydrogen with Pd containing alumina precipitates prepared by internal oxidation. The dissolved H was employed as a probe for the ceramic/metal interfaces. Their research concentrated on the low hydrogen content region where hydrogen is trapped both irreversibly and reversibly at the interface. The irreversibly held hydrogen was shown to be bonded to unsaturated oxygen atoms at the interface forming an interfacial monolayer which could be removed by evacuation at $T \geq 573$ K. The reversibly held hydrogen could be removed at about 423 K and was assumed to originate from a combination of segregation to the stress fields of the precipitates and interaction with chemical species at the interface [19]. Their measurements were carried out electrochemically at 295 K; the hydrogen chemical potential was monitored from the EMFs using the Pd containing Al_2O_3 precipitates as one and a saturated calomel as the other electrode. The upper limit of the hydrogen contents in their study was about H/Pd= r =0.01 [20]. Hydrogen solubilities in internally oxidized Pd–Mg, Pd–Zr and Pd–Zn alloys were also investigated by these authors in order to determine the strongly trapped hydrogen at the interfaces [19].

Gegner [21] has recently employed the internal oxidation of Pd–Fe alloys to determine the diffusion constant of dissolved oxygen in Pd, D_O. These alloys met his criteria of a well-defined internal oxidation front and the diffusion constant of Fe is quite small in comparison to D_O making the analysis simpler.

Noh et al. [22] have recently shown that after internal oxidation of a $Pd_{0.97}Al_{0.03}$ alloy, its complete hydrogen isotherm corresponds to one of pure Pd and it was shown that after partial internal oxidation, the H_2 isotherm consisted of two parts: one corresponding to pure Pd–H and the other to the $Pd_{0.97}Al_{0.03}$ alloy and therefore hydrogen isotherms can be used to determine the fraction of internal oxidation which occurred.

In the present study Fe will be internally oxidized resulting in iron oxide precipitates Pd within or $Pd_{0.77}Ag_{0.23}$ matrices. Strong traps for H at the Pd/oxide can be determined from measurement of H_2 isotherms because they will be characterized by large negative enthalpies and correspondingly negative H chemical potentials, $\mu_H = (1/2)RT\ln p_{H_2} + (1/2)\mu^\circ_{H_2}$, in comparison to the well-established H_2 solubility in Pd.

2. Experimental

Alloys were prepared by arc-melting the pure elements under argon. The buttons were flipped and re-melted several times. They were then annealed *in vacuo* for 3 days at 1133 K, rolled into foil and then re-annealed for 2 days at 1133 K. These alloys form solid solutions over the range to be investigated, $X_{Fe} = 0$ to 0.15 [2,23]. The diffusion parameters were determined from the permeation through the alloy membranes with p_{up} at the desired value and $p_{down} = 0$ as described for Pd and Pd–Ag alloy membranes [10,24]. The equation employed for these boundary values is

$$J = \frac{D_H c_{up}}{d} \quad (3)$$

where d is the membrane thickness and D_H is a concentration-dependent diffusion constant, c_{up} is the upstream H concentration and J will be defined as positive. Most of the un-oxidized membranes were palladized, i.e., a layer of Pd black was electrochemically deposited onto the alloy membrane which is thin enough to not significantly change the thickness.

Some alloys were internally oxidized (IOed) at elevated temperature in the atmosphere. The % IO was determined by weight changes. It has been shown before that the oxide precipitate which forms from IO is Fe_2O_3 [21,25].

3. Results and discussion

3.1. Hydrogen isotherms

3.1.1. Pd–Fe alloys

Isotherms for a series of Pd–Fe alloys plotted as $p_{H_2}^{1/2}$ against r are shown in Fig. 1 (473 K) where r =H-to-metal, atom ratio. At a fixed p_{H_2} in the dilute region the solubilities are seen to decrease with increase of X_{Fe} as expected for a contracted alloy system [1]. Under the conditions of the experiments, $T \geq 423$ K and $p_{H_2} \leq 1$ bar H_2(g), hydride phases do not form in these alloys.

Fig. 2 shows isotherms at different temperatures for a representative alloy, $Pd_{0.926}Fe_{0.074}$. It can be seen that there is considerable negative curvature indicating an H–H attractive interaction. ΔH_H and ΔS_H for H_2 absorption are determined from slopes and intercepts of plots of $\ln p^{1/2}$ against $1/T$ at constant r. ΔH_H values can be extrapolated to r =0 to obtain ΔH_H° and ΔS_H° is obtained from ΔS_H, using

$$\Delta S_H^\circ = \Delta S_H + R\ln\left(\frac{r}{1-r}\right) \quad (4)$$

and extrapolating ΔS_H° to $r = 0$ and it is assumed in the configurational partial entropy of Eq. (4) that all the octahedral interstices can be occupied. Results are shown in Table 1. There is seen to be a small decrease in $|\Delta H_H|$ at $X_{Fe} = 0.019$ and then it is nearly constant until it falls off at $X_{Fe} > 0.074$. ΔS_H° values are nearly constant

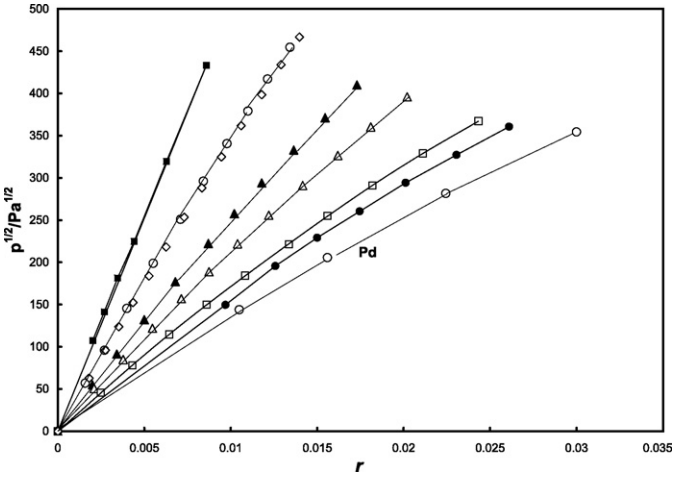

Fig. 1. Isotherms for a series of Pd–Fe alloys (473 K). ◯, Pd; •, $Pd_{0.981}Fe_{0.019}$; □, $Pd_{0.963}Fe_{0.037}$; △, $Pd_{0.0.944}Fe_{0.056}$; ▲; $Pd_{0.926}Fe_{0.074}$; ◯ and ◊, $Pd_{0.903}Fe_{0.097}$; ■, $Pd_{0.875}Fe_{0.125}$.

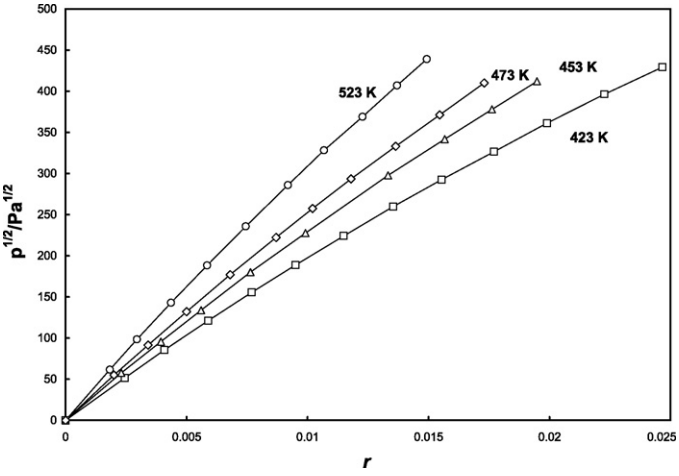

Fig. 2. Isotherms for the $Pd_{0.926}Fe_{0.074}$ alloys as a function of temperature.

at low X_{Fe} and then decrease with X_{Fe} indicating that interstices become blocked by nearest or next nearest neighbor Fe atoms, i.e., the assumption in Eq. (4) that all of the octahedral interstices are available is incorrect as reflected by the increasing values of $|\Delta S^{\circ}_{H}|$. For Pd–Ag alloys the same trend of ΔS° values is found although the trend of ΔH°_{H} with X_{Ag} is in the opposite direction [26].

From the regular interstitial solution model, we can write for small r [27]

$$RT\ln(p^{\frac{1}{2}}(1-r)/r) = \Delta H^{\circ}_{H} - T\Delta S^{\circ}_{H} + \mu^{E}_{H}(r) \approx \Delta H^{\circ}_{H} - T\Delta S^{\circ}_{H} + g_1 r \quad (5)$$

Table 1
Thermodynamics properties for H_2 solution (absorption) in homogeneous fcc Pd–Fe alloys (393–523 K) at infinite dilution of H; enthalpies are in units of kJ/mol $(1/2)H_2$, entropies J/K mol $(1/2)H_2$ and g_1 in kJ/mol $(1/2)H_2$ (473 K).

X_{Fe}	$-\Delta H^{\circ}_{H}$	$-\Delta S^{\circ}_{H}$	$-g_1$ (473 K)
0	8.2	52.0	43.5
0.019	8.5	51.6	40.2
0.037	8.6	52.1	38.8
0.056	8.1	53.0	36.7
0.074	8.2	54.5	37.5
0.097	6.7	53.9	24.7
0.125	6.2	55.6	–

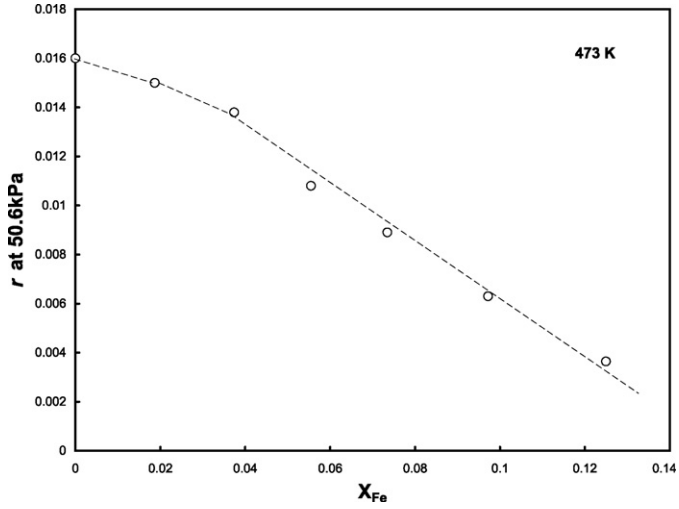

Fig. 3. H concentrations, r, at $p_{H_2} = 50.6$ kPa and 473 K for a series of Pd–Fe alloys.

where g_1 is the first order term in an expansion of $\mu^{E}_{H}(r)$ in r. A plot of the left-hand-side of Eq. (5) against r at a given temperature gives g_1 from the slope and $\Delta\mu^{\circ}_{H} = \Delta H^{\circ}_{H} - T\Delta S^{\circ}_{H}$ from the intercept [28]. The g_1 values obtained in this way are shown in Table 1 and they are seen to decrease slightly in magnitude with X_{Fe}.

Fig. 3 shows the H solubilities at 50.6 kPa and 473 K as a function of X_{Fe}. At low Fe contents it appears that there is not much change from Pd and at greater X_{Fe} values there is an almost linear fall-off with X_{Fe}. This reflects the behavior of ΔH°_{H} with X_{Fe}.

4. $(Pd_{0.77}Ag_{0.23})_{1-x}Fe_x$ alloys

Isotherms for the $(Pd_{0.77}Ag_{0.23})_{0.97}Fe_{0.03}$ and $(Pd_{0.77}Ag_{0.23})_{0.96}Fe_{0.04}$ alloys are shown in Figs. 4 and 5, respectively. It can be seen that the solubility is greater in the former compared to the latter. In Fig. 6 they are both compared at 473 K to an isotherm for the $Pd_{0.77}Ag_{0.23}$ alloy which is seen to have the greatest solubility, as expected. Thermodynamic parameters are shown in Table 2 for these ternary alloys as a function of r. ΔH_H becomes increasingly negative with r for the $(Pd_{0.77}Ag_{0.23})_{0.97}Fe_{0.03}$ alloy but is relatively constant for the $(Pd_{0.77}Ag_{0.23})_{0.96}Fe_{0.04}$ alloy. For comparison $\Delta H^{\circ}_{H} = -17(-18.0)$ kJ/mol H and $\Delta S^{\circ}_{H} = -54.1(-55.4)$ J/K mol H for the parent, binary alloy, $Pd_{0.77}Ag_{0.23}$, where the values without and with parenthesis were determined from plots of $\Delta\mu^{\circ}_{H}/T$ against $1/T$ and from plots of $\ln p^{1/2}$ against $1/T$ at different r val-

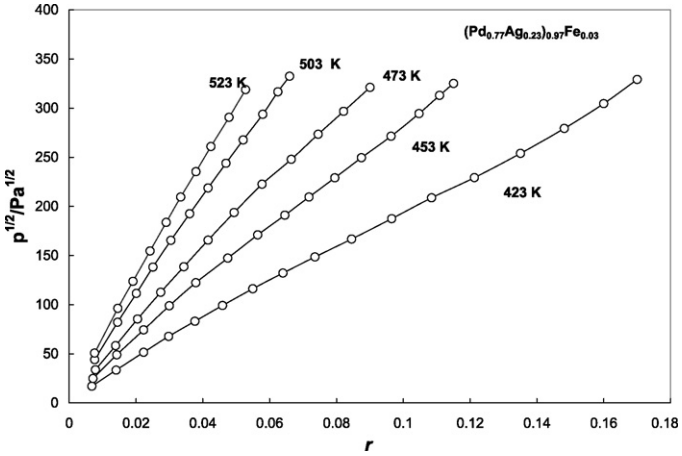

Fig. 4. Isotherms for a $(Pd_{0.77}Ag_{0.23})_{0.97}Fe_{0.03}$ alloy.

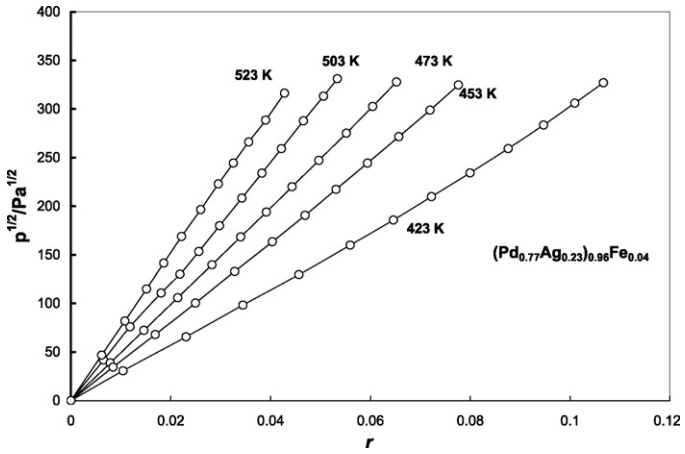

Fig. 5. Isotherms for a $(Pd_{0.77}Ag_{0.23})_{0.96}Fe_{0.04}$ alloy.

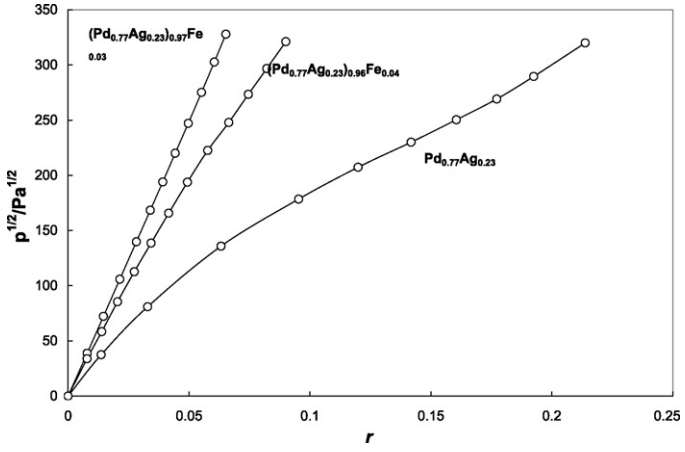

Fig. 6. Comparison of isotherms for $(Pd_{0.77}Ag_{0.23})_{0.96}Fe_{0.04}$ and $(Pd_{0.77}Ag_{0.23})_{0.97}Fe_{0.03}$ with the $Pd_{0.77}Ag_{0.23}$ alloy (473 K).

ues and then extrapolated to $r = 0$ [26]. It can be seen (Table 2) that ΔH°_{H}, the value at $r = 0$, for the $(Pd_{0.77}Ag_{0.23})_{0.97}Fe_{0.03}$ alloy is more negative than for the parent binary alloy which may reflect the slightly more negative value for the $Pd_{0.963}Fe_{0.037}$ alloy (Table 1), however, the value for the $(Pd_{0.77}Ag_{0.23})_{0.96}Fe_{0.04}$ alloy is similar to the binary alloy and therefore the results may be within experimental error. The ΔS°_{H} values differ presumably because of site blocking by both Ag and Fe.

Table 2
Thermodynamics of H_2 solution (absorption) in homogeneous fcc $(Pd_{0.77}Ag_{0.23})_{0.97}Fe_{0.03}$ and $(Pd_{0.77}Ag_{0.23})_{0.96}Fe_{0.04}$ (393–523 K) alloys as a function of r; enthalpies are in units of kJ/mol $(1/2)H_2$, entropies J/K mol $(1/2)H_2$.

r	$-\Delta H_H$	$-\Delta S^{\circ}_{H}$
$(Pd_{0.77}Ag_{0.23})_{0.97}Fe_{0.03}$		
0	−18.5	−61.2
0.01	−18.7	−61.2
0.02	−18.9	−61.2
0.03	−19.3	−61.7
0.04	−19.7	−61.0
0.06	−19.7	−61.8
0.08	−19.9	−61.6
$(Pd_{0.77}Ag_{0.23})_{0.96}Fe_{0.04}$		
0	−17.3	−59.2
0.02	−17.3	−59.0
0.03	−17.4	−59.3
0.04	−17.2	−59.3
0.05	−17.3	−58.8

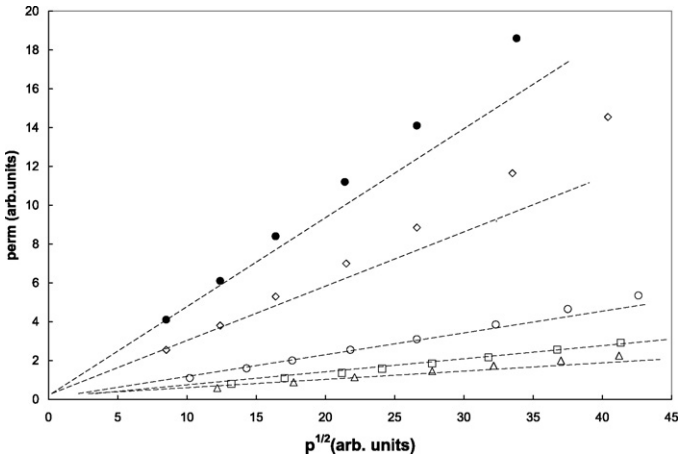

Fig. 7. H_2 permeabilities for a series of Pd–Fe alloys at 473 K. •, $Pd_{0.981}Fe_{0.019}$; ◊, $Pd_{0.963}Fe_{0.037}$; ○, $Pd_{0.903}Fe_{0.097}$; □, $Pd_{0.875}Fe_{0.125}$; △, $Pd_{0.85}Fe_{0.15}$ (503 K).

4.1. Diffusion parameters

4.1.1. Un-oxidized Pd–Fe alloys

Some permeabilities are shown as a function of $p_{up}^{1/2}$ in Fig. 7 where the various alloys are shown at 473 K except for the $Pd_{0.85}Fe_{0.15}$ alloy which is at 503 K. Such plots should be linear for systems in their ideal range of H contents which is seen to be the case for the $Pd_{0.85}Fe_{0.15}$ and $Pd_{0.875}Fe_{0.125}$ membranes where $D_H = D^*_H$ and $E_D = E^*_D$. The other alloys have contributions from non-ideality at higher $p_{up}^{1/2}$, i.e., higher r_{up}. The $Pd_{0.903}Fe_{0.097}$ alloy shows a small deviation from linearity and the $Pd_{0.963}Fe_{0.037}$ alloy shows larger deviations.

Specific permeabilities are shown in Table 3 for these Pd–Fe alloys at 473 and 423 K at $p_{up} = 50.7$ kPa and $p_{up} = 101.3$ kPa for the latter and at $p_{up} = 101.3$ kPa for the former temperature. Permeabilities depend on the product of the solubility and D_H at the p_{up} and temperature employed. Since both of these decrease with X_{Fe}, the permeabilities decrease. The decrease can be described approximately as an exponential fall with X_{Fe}.

Values of D^*_H (473 K) and E^*_D, the concentration-independent activation energy for diffusion, as a function X_{Fe} are shown in Fig. 8 where both have been determined by extrapolation to $r = 0$. In contrast to the expanded Pd–Ag alloys [24], D^*_H decreases continually starting from $X_{Fe} = 0$. This trend agrees with the findings of earlier workers [2,5,8] although the absolute magnitudes differ between the present work and the earlier work. The values of the pre-exponential factor, $D^{\circ,*}_H$ (Table 4), are all $(4.5 \pm 2) \times 10^{-3}$ cm^2/s except for the $Pd_{0.85}Fe_{0.15}$ alloy which is not very precise. Although there is no clear trend, the present values seem more reasonable than those reported for Pd–Fe alloys elsewhere, e.g., Sakamoto et al. report values in the range of 10^{-4} for the low Fe content alloys and then more reasonable values for the $Pd_{0.88}Fe_{0.12}$ and $Pd_{0.85}Fe_{0.15}$ alloys [2] whereas Yoshihara and McLellan [6] report

Table 3
Specific permeabilities for homogeneous fcc Pd–Fe alloys in units of (mol H/s cm^2)-cm.

X_{Fe}	473 K, $p_{up} = 101.3$ kPa	423 K, $p_{up} = 101.3$ kPa	423 K, $p_{up} = 50.7$ kPa
0	37.0×10^{-9}	24.2×10^{-9}	16.6×10^{-9}
0.019	26.4×10^{-9}	18.0×10^{-9}	11.9×10^{-9}
0.037	20.1×10^{-9}	13.7×10^{-9}	9.2×10^{-9}
0.074	10.2×10^{-9}	6.5×10^{-9}	4.3×10^{-9}
0.097	5.4×10^{-9}	3.1×10^{-9}	2.2×10^{-9}
0.125	3.4×10^{-9}	1.9×10^{-9}	1.7×10^{-9}
0.15	0.9×10^{-9}	1.0×10^{-9}	–

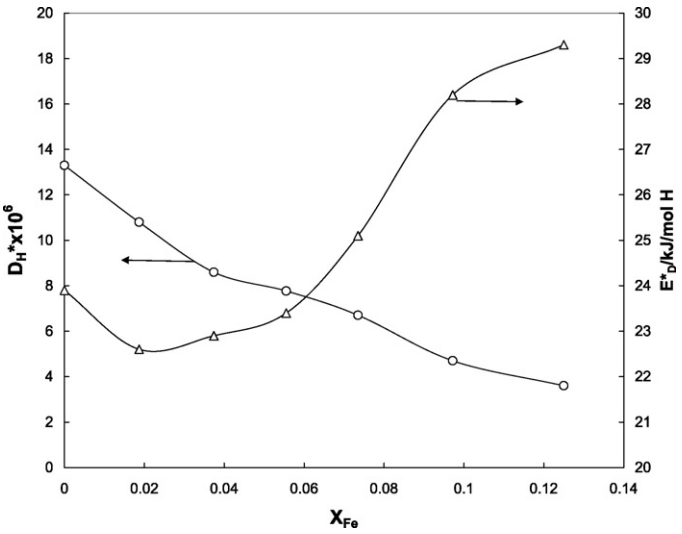

Fig. 8. D^*_H (473 K) and E^*_D for Pd–Fe alloys.

values increasing with X_{Fe} and for a $Pd_{0.89}Fe_{0.11}$ alloy $D^{\circ,*}_H = 1.79 \times 10^{-2}$ cm^2/s which seems to be anomalously large.

The E^*_D values lie between those found by [5,8] and by Sakamoto et al. [2]. The present higher temperature range will lead to smaller values of E^*_D [10]. In the present work E^*_D decreases slightly with X_{Fe} and then increases. Sakamoto et al. [2] find similar behavior at low Fe contents.

D_H was determined as a function of r at 423, 473 and 523 K for alloys with $X_{Fe} \leq 0.097$. In each case, D_H decreases with increase of r. For example, Fig. 9 shows a plot of RT ln D_H (473 K) and E_D against r for the $Pd_{0.963}Fe_{0.037}$ alloy. It has been shown elsewhere [10] that the slope of a RT ln D_H against r plot at low H contents is $\frac{1}{2}g_1$ and, as noted above, g_1 can also be determined from thermodynamic data. The slope of the data (Fig. 9) gives $g_1 = -25.8$ kJ/mol H as compared to −37.5 kJ/mol H from the thermodynamic results; it is not known what causes the large discrepancy, however, agreement is much better for the $Pd_{0.926}Fe_{0.074}$ alloy.

It has been shown for Pd–Ag alloys that E_D varies with r and the same is found for these Pd–Fe alloys except that the range of H contents over which E_D has been determined is smaller for these Pd–Fe alloys because of their more limited H_2 solubilities. For all of the Pd–Fe alloys investigated here, E_D increases with r. It has been shown elsewhere that at small r, the slope, $(dE_D/dr)_T$, is equal to $-\frac{1}{2}h_1$ [24] where $g_1 = h_1 - Ts_1$ (Eq. (5)) and for Pd–H, $h_1 < g_1$ [29]. For example, results are shown for the $Pd_{0.963}Fe_{0.037}$ alloy in Fig. 9 where the slope gives $h_1 = -100$ kJ/mol H and $h_1 = -82.5$ kJ/mol H for Pd–H [29] from thermodynamics, however, values from thermodynamics involve the temperature dependence of g_1 which is not very accurate.

Table 4
Diffusion parameters for homogeneous fcc Pd–Fe alloys (393–523 K) where D^*_H is in units of 10^{-6} cm^2/s, $D^{\circ,*}_H$ is in units of 10^{-3} cm^2/s and E^*_D and g_1 are in units of kJ/mol H.

X_{Fe}	D^*_H (extrap)(473 K)	E^*_D (extrap) ±1	$D^{\circ,*}_H$	g_1
0	13.3	23.9	5.6	–
0.019	10.8	22.6	3.4	−40.2
0.037	8.6	22.9	2.9	−20.6
0.056	7.8	23.4	3.0	−26.0
0.074	6.7	25.1	4.0	−37.5
0.097	4.7	28.2	6.1	–
0.125	3.6	29.3	6.2	–
0.15	3.5	30.7	8.6	–

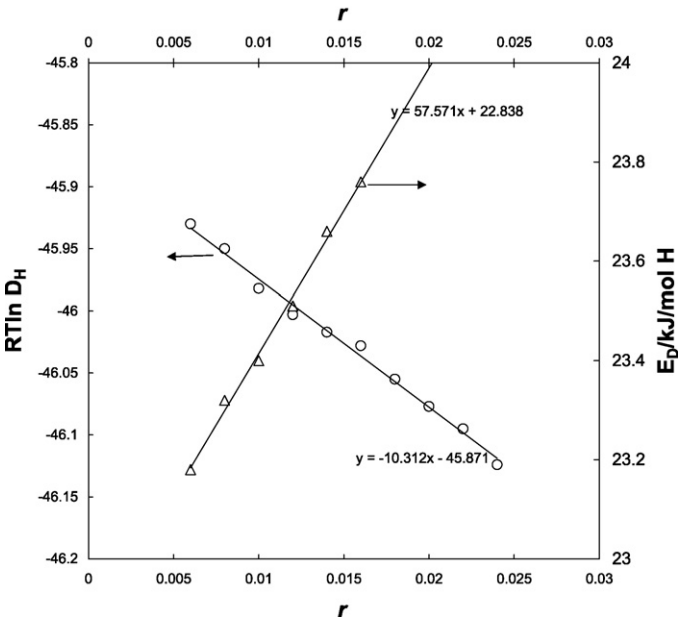

Fig. 9. Dependence of RTlnD_H and E_D on r for the $Pd_{0.926}Fe_{0.074}$ alloy (473 K).

4.1.2. Partially internally oxidized Pd–Fe alloys

Some permeation data were obtained for partially IOed alloys and because diffusion through the Pd layer resulting from the IO is faster than through the inner, un-oxidized Pd–Fe, the flux, J, is greater after IO. It has been shown by the authors that partial IO of Pd–Al alloys reduces the inhibition effect of CO on the H_2 permeation [15]. For this reason the effect of IO on the Pd–Fe alloys is of interest. The effect of CO on these H permeation through IOed alloy membranes will, however, be given elsewhere.

Fig. 10 shows for the $Pd_{0.926}Fe_{0.074}$ alloy (423 K) a plot of $1/J$ against $2d_{Pd}$ where the latter is determined from the % IO. The IO was carried out at 1073 K for times needed to attain the desired % IO. Similar plots were made earlier and for IOed Pd–Al alloys [30]. It is found here that the Pd–Fe alloys were less likely to leak due to cracking or pinholes after IO than the Pd–Al alloys. The plot is quite

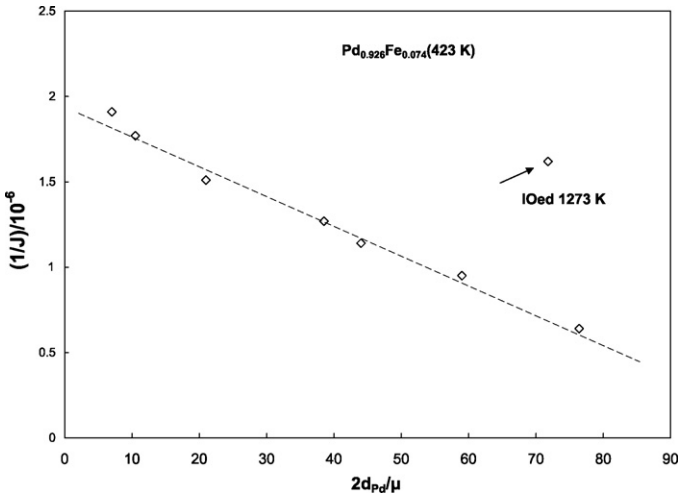

Fig. 10. $1/J$ plotted against the Pd thickness of a $Pd_{0.926}Fe_{0.074}$ membrane after various degrees of IO (423 K) where J has the units of (mol H/s)/cm^2.

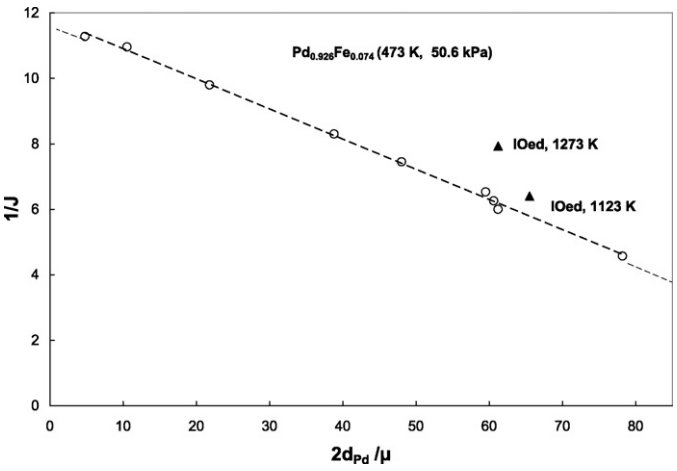

Fig. 11. $1/J$ plotted against the Pd thickness of a $Pd_{0.926}Fe_{0.074}$ membrane after various degrees of IO at 473 K where it J has the units of (mol H/s)/cm^2.

linear according to the following equation

$$\frac{1}{J} = \frac{Kd_o}{c_o D_{H,alloy}} + \frac{2d_{Pd}}{c_o}\left[\frac{1}{D_{H,Pd}} - \frac{K}{D_{H,alloy}}\right] \quad (6)$$

which was derived earlier [30]; c_o is the H concentration at the upstream side determined from p_{up}, d_o the total membrane thickness, d_{Pd} the thickness of each Pd layer after IO and is obtained from $2d_{Pd}$ = fraction IO × d_o and $K = 2.0$ is the ratio of the H contents at the interface of the Pd and the un-oxidized alloy which is known from isotherms for Pd and the alloy. The intercepts are $Kd_o/c_oD_{H,alloy}$ and $d_o/c_oD_{H,Pd}$ at $2d_{Pd} = 0$ and $2d_{Pd} = d_o$, respectively. The linear behavior (Fig. 10) shows clearly that the permeation is bulk diffusion-controlled for these alloys in these experiments.

Similar data are shown at 423 K in Fig. 11 where linear behavior is also seen. Several data points (Figs. 10 and 11) are given for alloys IOed at higher temperatures than the 1073 K employed for the data which falls on or near the lines. For example, some data were obtained after IO at 1273 K which deviate from the linear plot, i.e., the fluxes are much slower than for the data for IO at 1073 K. The reason for this may be that the larger oxide precipitates which form at the higher temperatures may form near the surface and tend to decrease the area available for permeation.

The permeation of a partially (16.3%) IOed $Pd_{0.963}Fe_{0.037}$ alloy was measured at different temperatures at $p_{up} = 50.6$ and 90.6 kPa and the Arrhenius plots are shown in Fig. 12 where the slopes are quite similar at the two p_{H_2} used for the permeation experiments.

The partially (16.3%) IOed $Pd_{0.963}Fe_{0.037}$ alloy membrane alloy was then fully hydrided and dehydrided (cycled) *in situ* at ambient temperature. The purpose of this was to determine how the permeability is affected by cycling. Specifically it can be determined whether there is any mechanical breakdown due to the abrupt volume changes accompanying the hydride phase change. The re-determined permeabilities are found to increase by about 20% at each p_{up} (Fig. 12), however, the slopes of the plots are similar before and after the cycling. It would be expected that any cracks or pinholes through the cycled membranes would be reflected by markedly different slopes and permeation rates. The small increase of permeability may be due to an increased membrane area from an increase of surface roughness and some cracking which does not penetrate the membrane. These results are of some interest because purification membranes have been avoided in the past because of the possibility of hydride phase formation and accompanying mechanical breakdown [31].

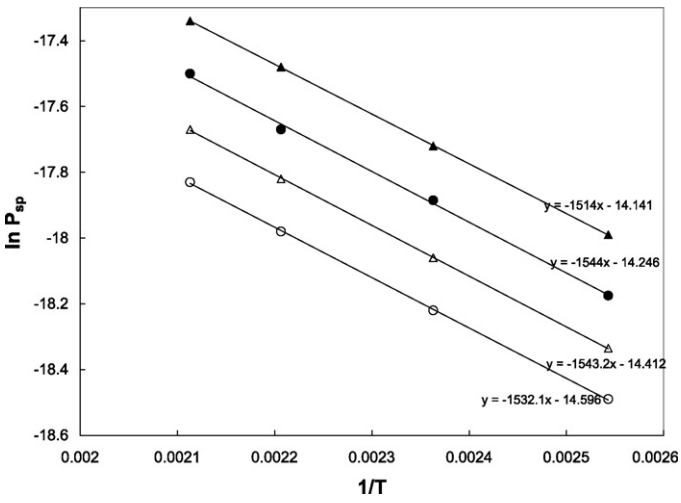

Fig. 12. Arrhenius plots of the specific permeability for a $Pd_{0.963}Fe_{0.037}$ alloy membrane. ○, IOed 16.2%, 50.6 kPa: △, same conditions except at 90.6 kPa; •, cycled, IOed 16.2%, 50.6 kPa: ▲, same conditions except at 90.6 kPa.

4.1.3. Partially internally oxidized $(Pd_{0.77}Ag_{0.23})_{1-x}Fe_x$ alloys

Diffusion constants were determined for these ternary alloys with $x = 0.03$ and 0.04 using partially IOed alloys and plots of $1/J$ versus % IO as shown in Figs. 13 and 14. These diffusion constants are for r_{up} corresponding to p_{up}=50.6 kPa at 473 K and are shown in Table 5. The diffusion constants are determined from the intercepts of the plots in Figs. 13 and 14 according to Eq. (6). The diffusion constants are seen to be smaller in the ternary alloys than in the parent alloy and the diffusion constant for the $X_{Fe} = 0.03$ alloy is greater than for the 0.04 alloy.

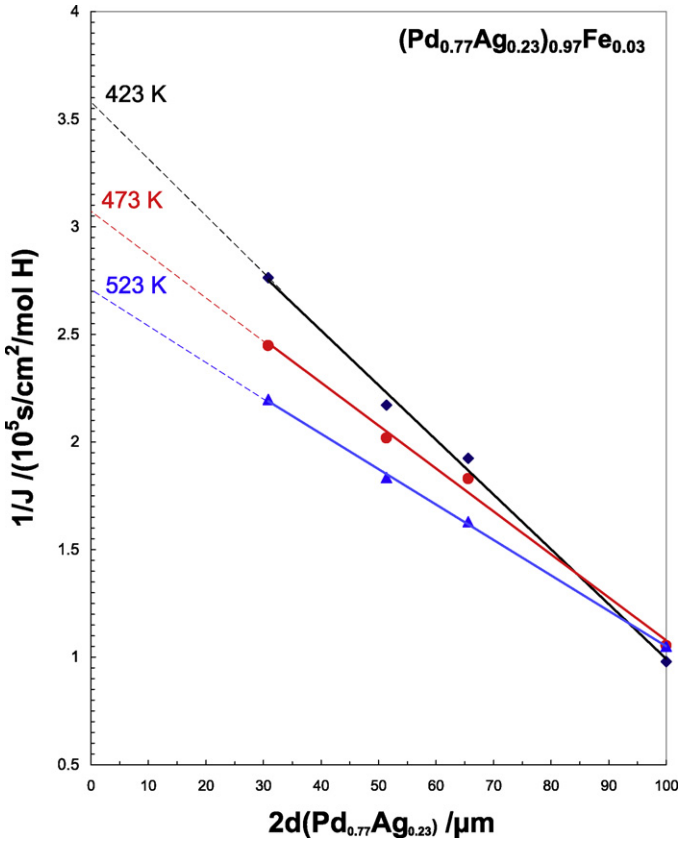

Fig. 13. $1/J$ plotted against the Pd thickness of a $(Pd_{0.77}Ag_{0.23})_{0.97}Fe_{0.03}$ membrane after various degrees of IO at 473 K.

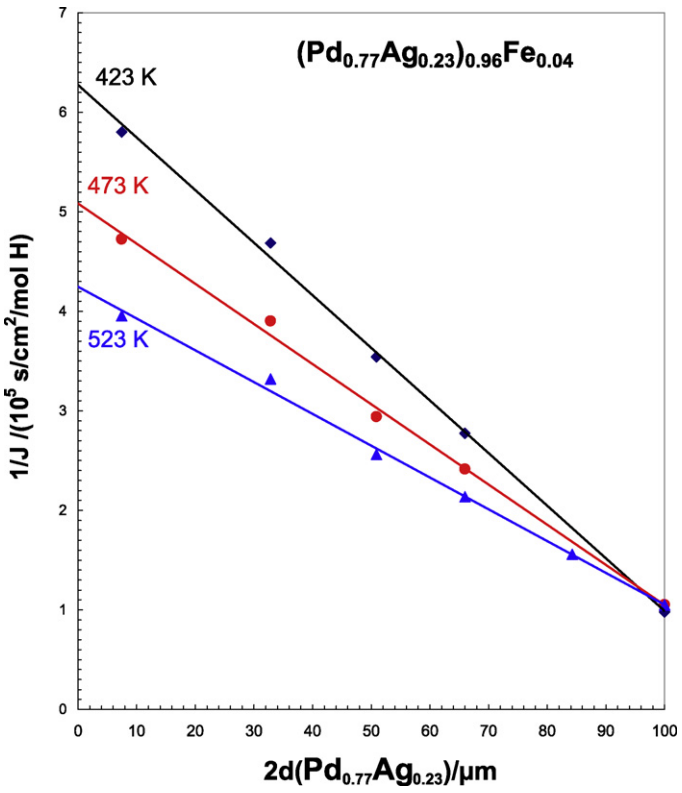

Fig. 14. $1/J$ plotted against the Pd thickness of a $(Pd_{0.77}Ag_{0.23})_{0.96}Fe_{0.04}$ membrane after various degrees of IO of a $Pd_{0.926}Fe_{0.074}$ alloy (473 K).

Table 5
Diffusion parameters for homogeneous fcc $(Pd_{0.77}Ag_{0.23})_{1-x}Fe_x$ alloys where D_H is in units of cm^2/s.

T (K)	D_H at $p_{up} = 50.6$ kPa		
	$Pd_{0.77}Ag_{0.23}$	$(Pd_{0.77}Ag_{0.23})_{0.97}Fe_{0.03}$	$(Pd_{0.77}Ag_{0.23})_{0.96}Fe_{0.04}$
423	13.0×10^{-6}	9.4×10^{-6}	7.2×10^{-6}
473	6.6×10^{-6}	5.1×10^{-6}	4.0×10^{-6}
523	3.4×10^{-6}	2.2×10^{-6}	1.9×10^{-6}

5. Conclusions

From the equilibrium isotherms, thermodynamic properties have been determined (423–523 K) for a series of Pd–Fe alloys and the relative partial molar enthalpies for H_2 absorption increase and the standard relative partial molar entropies decrease with X_{Fe}. These results support the earlier lower temperature results [5] rather than [2]. In the dilute phase region the H_2 solubilities decrease with X_{Fe} at a given p_{H_2} as expected for contracted alloys [1].

Diffusion parameters have been determined and, as r increases, D_H and E_D decrease and increase in value with r, respectively. In contrast with previous results [2,6], $D_H^{*,\circ}$ remains at $4.5 \pm 2.0 \times 10^{-3}$ cm^2/s except for the $Pd_{0.875}Fe_{0.125}$ alloy which is probably within experimental error. Diffusion through partially IOed alloys has been investigated and a linear correlation has been found between $1/J$ and the thickness of oxidized alloy which shows that bulk diffusion control is the slow step. An IOed alloy membrane was hydrided/dehydrided and subsequently the permeability was slightly faster with no evidence of any deleterious effect of the cycling on the membrane.

References

[1] Y. Sakamoto, F. Chen, M. Ura, T. Flanagan, Ber. Bunsenges Physik. Chem. 99 (1995) 807.
[2] Y. Sakamoto, T. Ohishi, E. Kumashiro, K. Takao, J. Less-Common Met. 88 (1982) 379.
[3] J. Carlow, R. Meads, J. Phys. F: Met. Phys. 2 (1969) 2120.
[4] W. Zhang, S. Luo, T. Flanagan, J. Alloys Compd. 291–295 (1999) 1.
[5] T. Flanagan, G. Gross, J. Clewley, 2nd International Congress on Hydrogen in Metals, vol. VI, Paris, France, 1977.
[6] M. Yoshihara, R. McLellan, Acta Metall. 30 (1982) 1605.
[7] M. Yoshihara, R. McLellan, J. Phys. Chem. Solids 47 (1986) 225.
[8] R. McLellan, L. Yang, Scr. Metall. Mater. 30 (1994) 155.
[9] E. Wicke, H. Brodowsky, G. Alefeld, J. Völkl, in: Hydrogen in Metals, II, Springer-Verlag, Berlin, 1978.
[10] T. Flanagan, D. Wang, K. Shanahan, J. Membr. Sci. 306 (2007) 66.
[11] H. Wipf, in: Hydrogen in Metals, III, Springer-Verlag, Berlin, 1997.
[12] Y. Fukai, The Metal–Hydrogen System, Springer-Verlag, Berlin, 2005.
[13] R. Kirchheim, R. McLellan, Acta Metall. 28 (1980) 1549.
[14] H. Barlag, L. Opara, H. Züchner, J. Alloys Compd. 330–332 (2002) 434.
[15] D. Wang, T. Flanagan, K. Shanahan, J. Membr. Sci. 253 (2005) 165.
[16] D. Wang, T. Flanagan, Scr. Mater. 56 (2007) 261.
[17] J. Eastman, M. Rühle, Ceram. Eng. Sci. Proc. 10 (1989) 1515.
[18] X. Huang, W. Mader, J. Eastman, R. Kirchheim, Scr. Mater. 22 (1988) 1109.
[19] X. Huang, W. Mader, R. Kirchheim, Acta Metall. Mater. 39 (1991) 893.
[20] R. Kirchheim, X. Huang, T. Mütschele, N. Moody, A. Thompson (Eds.), Metal–Hydrogen Systems, The Minerals, Metals and Materials Society D, 1990, p. 85.
[21] J. Gegner, PhD Thesis, University Stuttgart, 1995.
[22] H. Noh, T. Balasubramaniam, R. Balasubramaniam, J. Eastman, Scr. Mater. 34 (1996) 863.
[23] M. Hansen, Constitution of Binary Alloys, McGraw-Hill, New York, 1958.
[24] D. Wang, T. Flanagan, K. Shanahan, J. Phys. Chem. B 112 (2008) 1135.
[25] D. Wang, T. Flanagan, R. Balasubramaniam, J. Alloys Compd. 356–357 (2003) 3.
[26] T. Flanagan, D. Wang, S. Luo, J. Phys. Chem. B 111 (2007) 10723.
[27] W. Oates, T. Flanagan, J. Mater. Sci. 16 (1981) 3235.
[28] T. Flanagan, W. Oates, Ann. Rev. Mater. Sci. 21 (1991) 269.
[29] T. Kuji, W. Oates, B. Bowerman, T. Flanagan, J. Phys. F: Met. Phys. 13 (1983) 1785.
[30] D. Wang, T. Flanagan, K. Shanahan, Scr. Mater. 54 (2006) 1317.
[31] F. Lewis, The Palladium–Hydrogen System, Academic Press, New York, 1967.